Int J Adv Manuf Technol (2017) 88:2717–2725
DOI 10.1007/s00170-016-8802-2

ORIGINAL ARTICLE

Analysis of process parameter effects during narrow-gap triple-wire gas indirect arc welding

Disheng Fang[1] · **Liming Liu**[1]

Received: 2 December 2015 / Accepted: 18 April 2016 / Published online: 8 June 2016

Abstract Narrow-gap triple-wire gas indirect arc (TW-GIA) welding is a novel process. Previous studies have reported the process and explained how the wire arrangement affects the arc behavior and the metal transfer which correspondingly affect the sidewall fusion. In this paper, effects of process parameters on sidewall fusion, weld bead formation, microstructure, and hardness are studied, to reveal more characteristics of the narrow-gap TW-GIA. Results show that welding currents affect the sidewall penetration more significantly than groove gap and welding speed. In addition, sidewall penetration increases with larger welding currents. The heat affected zone (HAZ) width decreases with lower welding current, wider groove gap, or higher welding speed. With all the parameters, weld beads produced by narrow-gap TW-GIA present convex surfaces, which can lead to serious incomplete fusion at the weld root for the next weld layer. To solve this problem, addition of a gas tungsten arc (GTA) behind the TW-GIA is proposed. An additional benefit is that the arc pressure and extra heat input of the GTA obtain weld beads with concave surfaces.

Keywords Narrow-gap · Welding · Weld bead formation · Indirect arc · Sidewall fusion

✉ Liming Liu
liulm@dlut.edu.cn

[1] Key Laboratory of Liaoning Advanced Welding and Joining Technology, School of Materials Science and Engineering, Dalian University of Technology, Dalian 116024, China

1 Introduction

Narrow-gap gas metal arc welding (GMAW) possesses obvious advantages for welding thick metals, compared to traditional GMAW process [1]. Firstly, it improves productivity significantly because less deposit metals are needed with I groove type [2]. Second, it is usually conducted with low heat input, producing weld joints with less deformation and more desirable mechanical performance [3]. Currently, various narrow-gap GMAWs have been developed and studied, such as rotating arc narrow-gap GMAW [4] and double wire narrow-gap GMAW [5]. Their focuses are on the sidewall fusion, because sidewall fusion is the key problem for narrow-gap welding [6]. Weld bead formation is another focus for studying narrow-gap welding, because it is very difficult to produce complete fusion at the weld root for the next weld layer if a convex weld bead surface is formed. A concave weld bead is more beneficial [7].

Based on twin-wire indirect arc welding [8], triple-wire gas indirect arc (TW-GIA) is proposed as a novel process [9]. During TW-GIA, two power supplies are connected among three wires, and electric arc establishes between the wires. The base material conducts no electric currents, and it is heated by the indirect arc column and the metal transfer. TW-GIA has the advantages such as high melting efficiency, low heat input, low welding deformation, and low penetration ratio. Narrow-gap TW-GIA welding process is obtained by applying TW-GIA with a specific wire arrangement [10]. Previous studies have reported the process and explained how the wire arrangement affects the arc behavior and the metal transfer which correspondingly affect the sidewall fusion. A particular wire arrangement is configured for narrow-gap TW-GIA.

In this paper, effects of the process parameters on sidewall penetration, weld bead formation, and microstructures are analyzed, to reveal more characteristics of narrow-gap TW-GIA welding [11]. Because the weld bead forms a convex surface with TW-GIA in narrow-gap welding which poses a great challenge for the second weld layer, addition of a gas tungsten arc (GTA) behind the TW-GIA is proposed. The effect of the GTA on the weld bead formation and microstructure is preliminarily studied.

2 Principle and experimental procedures

Figure 1 presents the principle of the narrow-gap TW-GIA welding. It shows that there are two power supplies and triple wires in this system. The power supplies are connected through three wires, and the base material does not link to the power supply. Cathodes of the power supplies are connected to one wire which is called the main wire, and the anodes are connected to the other wires which are called side wires. During welding, the currents that the three wires carry are I_1, I_2, and I, respectively, and the current I equals I_1 plus I_2. For narrow-gap welding, base materials are steel plates with geometry of $300 \times 150 \times 20$ mm^3, and they are configured with I groove type. In the figure, *d* represents the groove gap distance. Ceramic backing is used for weld bead formation at the back side.

Figure 2 presents the wire arrangement to achieve effective sidewall fusion according to previous studies. In the figure, the main wire tilts 45° from horizontal level, and the side wires keep a 30° angle with the main wire. Three wires intersect at one spot. The main wire is in the middle, and the side wires deviate from the main wire in opposite directions. But the side wires are still in contact with the main wire to establish an electric arc.

For the actual welding experiment, base materials are low carbon steel (Q235), and the welding wire is ER50-6. The diameter of the main wire is 1.6 mm, and the side wires are 1.2 mm. Nominal chemistry compositions of the base material and the welding wires are given in Table 1. Shielding gases are mixture gases of 80 % CO_2 and 20 % Ar, and the shielding gas

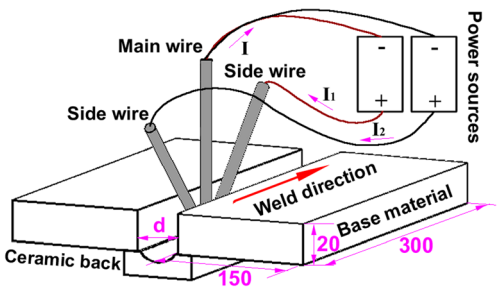

Fig. 1 Principle of the narrow-gap triple-wire indirect arc welding

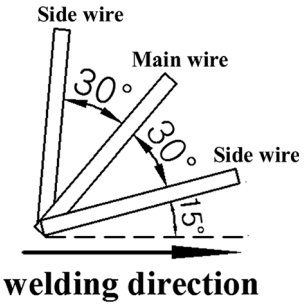

Fig. 2 Wire arrangement of narrow-gap triple-wire indirect arc

flows out from a gas nozzle which is placed above the indirect arc during welding. After welding, the weld bead is cross-sectioned, and then, the specimen is ground with different grades of emery cloth, polished with 1-μm diamond paste, and etched by 4 % nitric acid. The geometry of the weld bead is measured on the captured image of the cross-section with computer software. The microstructure is observed with an optical microscope. Vickers micro-hardness is tested with 200 N of load and 15 s of dwell time. At last, integration of gas tungsten arc (GTA) with TW-GIA is proposed, and its effect is preliminarily discussed by comparing the welding results with and without the GTA.

3 Results and discussion

3.1 Effect of parameters on weld bead formation

Figure 3 shows the schematic diagram of a typical weld bead cross-section with narrow-gap TW-GIA welding. In the figure, *T*, *R*, *W*, *P*, and *H* represent the total thickness of the weld bead, convex height, total width of the weld bead, sidewall penetration, and width of the heat affected zone, respectively. The FZ, HAZ, and the BM are the acronyms for fusion zone, heat affected zone, and base materials, respectively. The parameters to be studied are welding current, groove gap, and welding speed.

While other parameters remain constant (groove gap 10 mm, welding speed 600 mm/min), weld beads with different total average currents (the current that the main wire carries) are presented in Fig. 4. Figure 4a, b, c, d is the weld bead by 280, 320, 400, and 480 A, respectively. Figure 7a

Table 1 Nominal chemical composition (wt.%) of the base material and welding wires

Materials	C	Mn	Si	S	P	Cr	Cu	Fe
Base metal Q235	0.17	0.46	0.26	0.007	0.009	0.02	–	Bal.
Welding wire ER50-6	0.10	1.54	0.90	0.020	0.018	–	0.10	Bal.

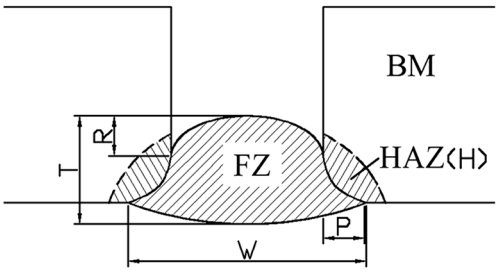

Fig. 3 Schematic diagram of the weld bead cross-section

shows the measured geometric values of the weld bead. From Figs. 4 and 7a, the main conclusions drawn are as follows: the side wall penetration increases as the welding current increases; therefore, the possibility for incomplete sidewall fusion is reduced. In addition, the HAZ width increases with higher welding current. The reason for this is that the temperature of the indirect arc and the metal droplet increases as the welding current improves [12]. The weld bead thickness increases with higher currents due to increasing wire melting rate. The weld beads form convex surfaces, and the convex height has no obvious change with different currents. From previous study, it is learned that the melting rate of the main wire is always two times larger than the side wires. And the metal droplet of the main wire transfers along the main wire in the middle of the weld bead, while the droplet of the side wires is repelled to the sidewall. As a result, a convex bead surface is formed. During the process, total average currents lower than 280 A are not employed because the stability worsens as the metal transfer shifts from spray transfer to globular metal transfer at lower currents than 280 A.

Weld beads with different groove gaps are presented in Fig. 5, while other parameters remain constant (total average current 480 A, welding speed 600 mm/min). Figure 5a, b, c, d is in accordance to 8, 10, 12, and 14 mm, respectively. The measured geometric values of the weld beads are shown in Fig. 7b. From the Figs. 5 and 7b, the following conclusions are drawn: the sidewall penetration does not vary too much at different groove gaps, but the HAZ is narrower with a wider groove gap. During narrow-gap TW-GIA welding, the base material melts because of the heat input from the indirect arc and metal transfer. And during thermal cycle, the heating rate is much higher than the cooling rate. Because of the high heating rate, the base material can be similarly melted within a certain range of heat input [13]. However, the dwelling time over the peak temperature is shorter with a lower heat input. The weld bead surface is wider with a wider groove gap leading to faster cooling rate. As a result, a narrower HAZ is reached with a wider groove gap. All the weld beads have convex surfaces, and the convex height does not change much at varied groove gap. Total weld bead thickness decreases with wider groove gap. A narrower gap distance is believed to be more beneficial for the narrow-gap welding, but the stability is not good when the gap distance is at 8 mm in the present experiment.

While keeping the other parameters constant (total average current 480 A, groove gap 10 mm), weld beads with different welding speed are presented in Fig. 6. Figure 6a, b, c, d corresponds to 500, 600, 700, and 800 mm/min, respectively. The measured geometric values of the weld beads are shown in Fig. 7c. The main conclusions are as follows: total width and sidewall penetration change little as the welding speed varies. The HAZ width decreases with faster welding speed; the reason is similar to the explanation for the groove gap. When the welding speed is too high at 800 mm/min, there is obvious

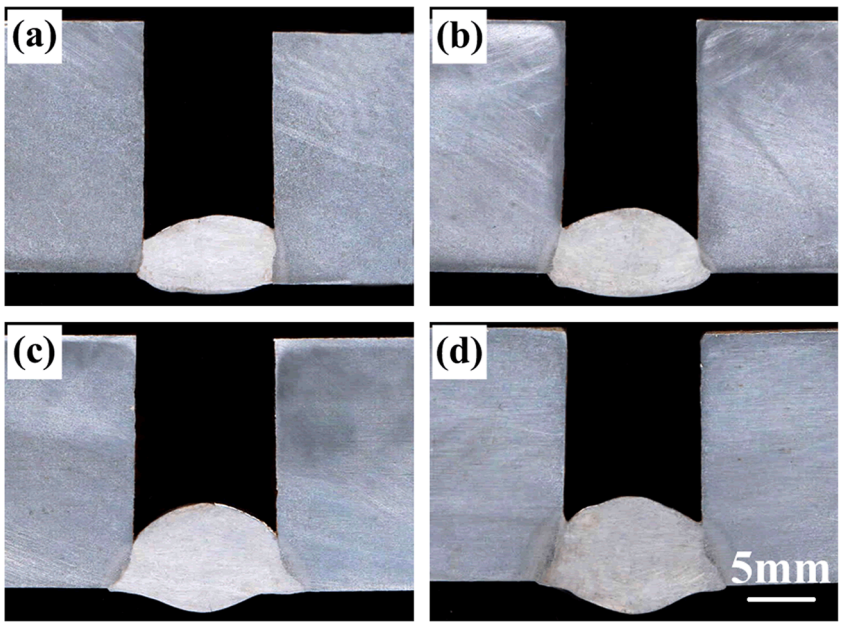

Fig. 4 Weld beads with different total average currents; **a**, **b**, **c**, and **d** correspond to 280, 320, 400, and 480 A, respectively

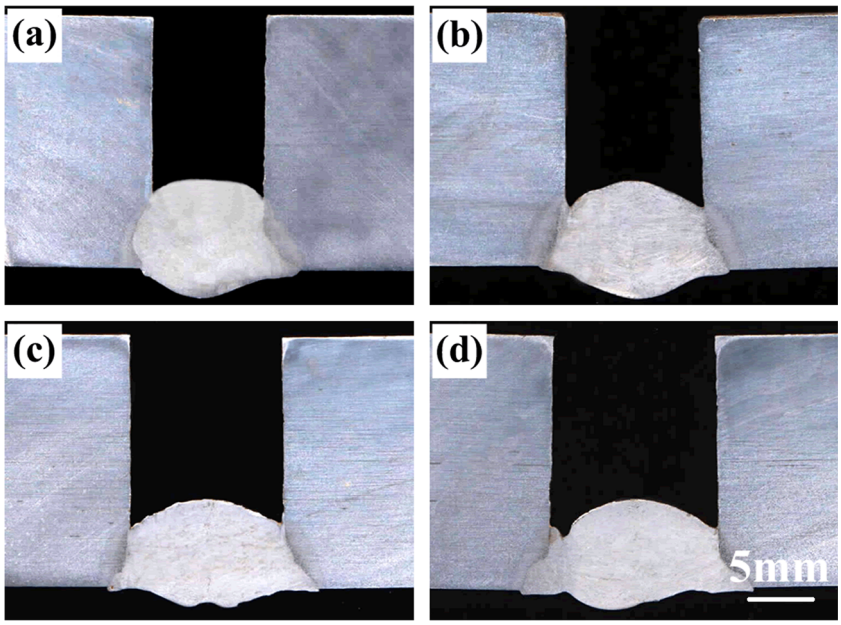

Fig. 5 Weld beads with different groove gap; **a**, **b**, **c**, and **d** correspond to 8, 10, 12, and 14 mm, respectively

undercut because the melted metal does not fill the weld bead sufficiently. The convex weld bead formation cannot be eliminated by varying the welding speed.

3.2 Effect of welding currents on microstructure and hardness

Microstructure of the weld beads in the FZ with various welding currents is shown in Fig. 8. Figure 8a, b, c, d is in accordance with 480, 400, 320, and 280 A, respectively. It shows that all the images consist of columnar grains, and these grains are made of ferrite and small proportions of pearlite and cementite. The width of the columnar grain is around 58 ~ 230 μm with current 480 A, 32 ~ 165 μm with current 400 A, 54 ~ 101 μm with current 320 A, and 28 ~ 170 μm with current 280 A, respectively. Apparently, as the welding current gradually decreases, the grain size gradually becomes smaller. When the current is at 280 A, the columnar grain tends to become equiaxed grain. Because the chemical composition is similar for all the weld beads, the above microstructure difference is caused by varied heat input. As the heat input decreases with lower welding currents, the crystal grain has less time to grow during solidification; therefore, it has a smaller grain size.

Microstructure of the weld beads in the HAZ with varied welding currents is shown in Fig. 9. And Fig. 9a, b, c, d

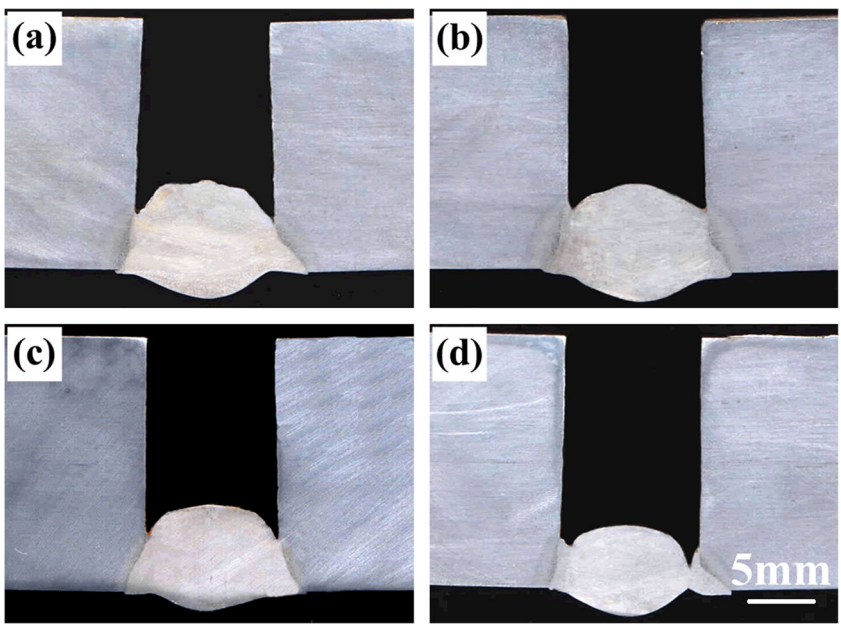

Fig. 6 Weld beads with different welding speeds; **a**, **b**, **c**, and **d** correspond to 500, 600, 700, and 800 mm/min, respectively

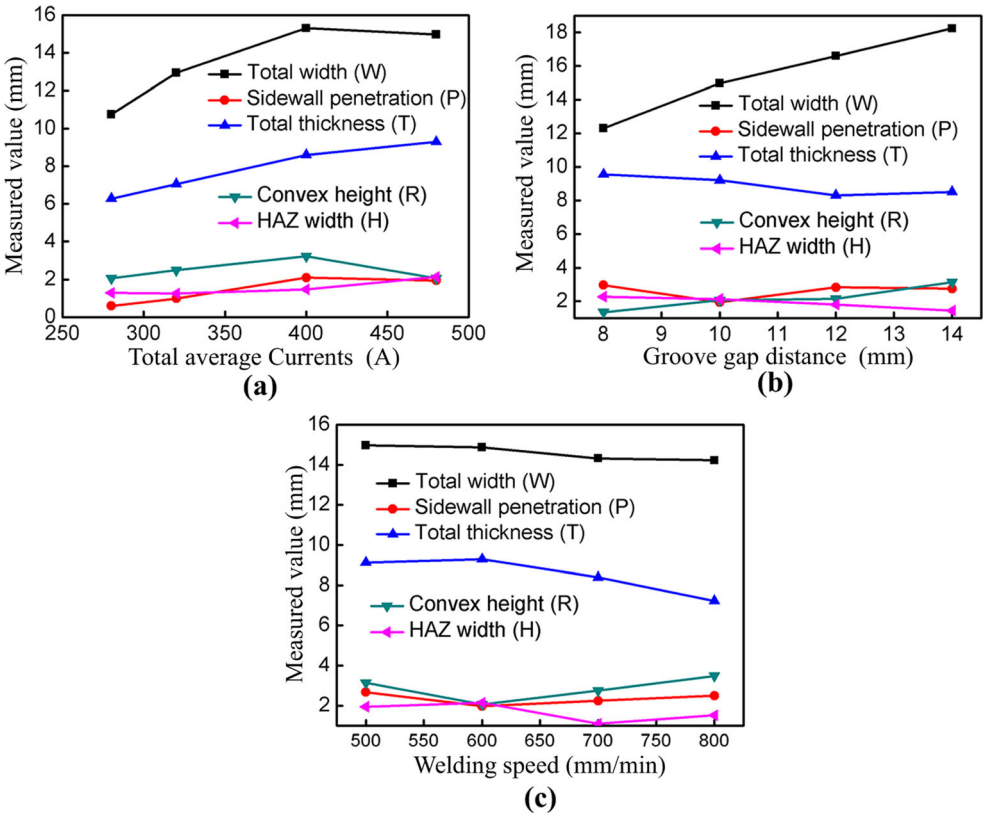

Fig. 7 Geometry of weld beads with different process parameters; **a** total average currents, **b** groove gap, **c** welding speed

is in accordance with 480, 400, 320, and 280 A, respectively. The figure shows that the microstructure of the HAZ mainly consists of ferrite and pearlite. In Fig. 9a, there are obvious coarse grains on the left side of the image, when the welding current at 480 A, and the coarse grain size is about 95 ~ 150 μm. But in Fig. 9b, c, d, the coarse grains gradually become fewer and smaller, as the welding current decreases. Especially when the welding current is at 320 and 280 A, there is no obvious coarse grain in the HAZ. As the heat input decreases with lower welding currents, the peak temperature of the thermal cycle becomes lower, and materials stay a shorter time above the effective

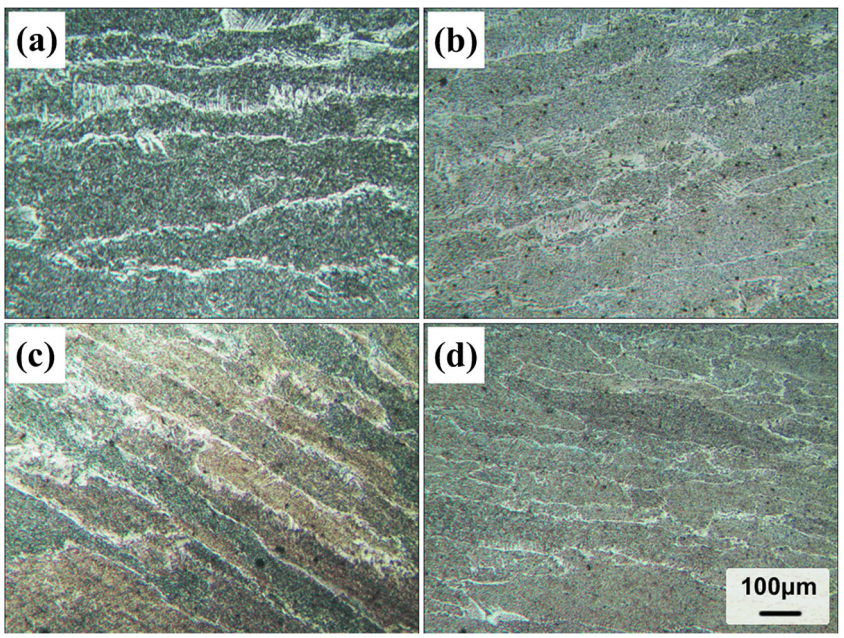

Fig. 8 Microstructure at the FZ with different welding current; **a**, **b**, **c**, and **d** are in accordance to 480, 400, 320, and 280 A, respectively

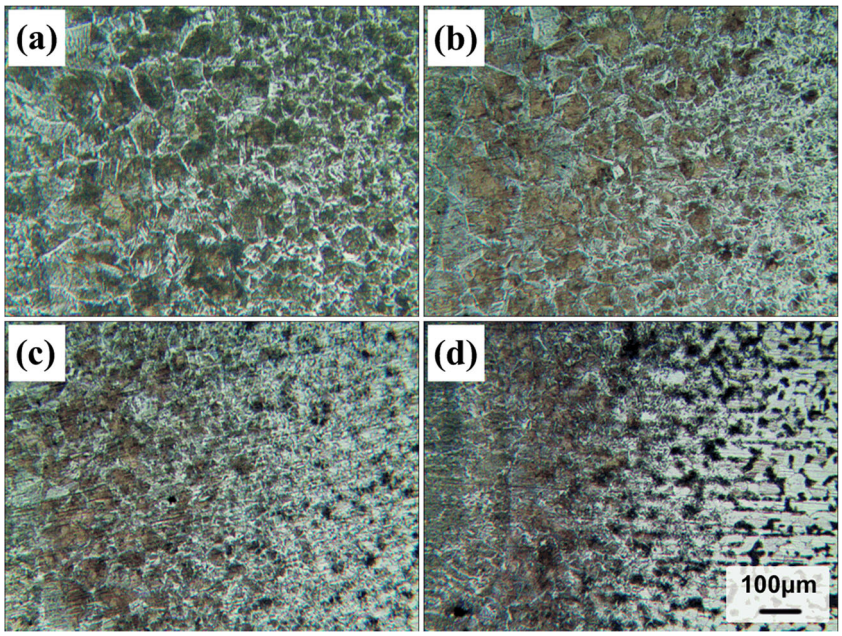

Fig. 9 Microstructure at the HAZ with different welding current; **a**, **b**, **c**, and **d** are in accordance to 480, 400, 320, and 280 A, respectively

recrystallization temperature [14]. As a result, the diffusion takes place within shorter time, leading to narrower HAZ and smaller grain size.

Hardness distribution of the weld beads with different welding currents is shown in Fig. 10. Figure 10a, b, c, d is in accordance with 480, 400, 320, and 280 A, respectively. It shows that the hardness of the HAZ is greater than that of the base material and the FZ has the highest hardness of all the weld beads. In the FZ, the hardness increases when the welding current decreases; for example in Fig. 10a, the highest hardness is 235.1 HV, and in Fig. 10d, the highest hardness is 257.9 HV. Heat input is smaller due to lower welding current, leading to faster cooling rate. As a result, microstructure tends to grow hard and brittle [15]. This discussion shows that the microstructure and the hardness are strongly associated with the heat input, and the heat

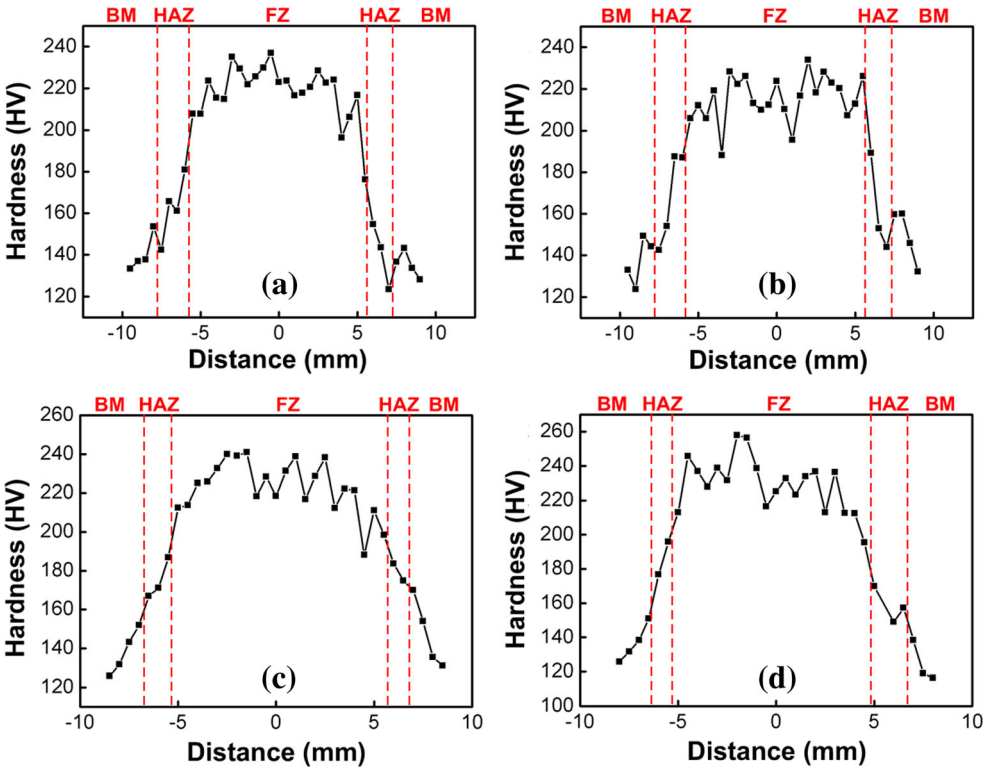

Fig. 10 Hardness distribution of the weld bead with different currents; **a**, **b**, **c**, and **d** are in accordance to 480, 400, 320, and 280 A, respectively

Table 2 Welding parameters of the TW-GIA

Power sources	(Base-pulse) current	Voltage	Pulse frequency	Pulse time	Side wire feed rate	Main wire feed rate
Pulsed-DC	145–295 A	–	140 Hz	2.8 ms	7.3 m/min	12.0 m/min
DC	203 A	29.2 V	–	–	7.2 m/min	

input is indicated by the HAZ width. Because the base material is a very common kind of steel, the microstructure and hardness of the weld beads with other parameters are not presented explicitly.

3.3 Proposal of integrating a gas tungsten arc in TW-GIA

3.3.1 Effect of the GTA on weld bead formation

When the GTA is added, it is placed 10 mm behind the wire intersection of the TW-GIA. The current of the GTA is 200 A in the root layer and is 300 A in the second layer. With and without the GTA, the TW-GIA employed the same parameters which are listed in Table 2 for comparison. Welding speed for the root layer is 600 mm/min, and for the second layer, it is 750 mm/min; the groove gap is 10 mm.

Figure 11 shows the welding results with and without the GTA behind the TW-GIA. Figure 11a, c is the weld bead without the GTA. Figure 11a is only the root layer, and Fig. 11c is with a second layer. They show that the weld beads have convex surfaces, and there is incomplete fusion at the weld root of the second layer. Also, the fusion between the root layer and the second layer is incomplete.

Figure 11b, d is welding result with a GTA behind the TW-GIA. Figure 11b is the root layer, and it shows that the weld bead presents a concave surface. In Fig. 11d, a second layer is conducted, and it shows that complete fusion at the weld root of the second layer, and complete fusion between the two weld layers are achieved. Comparing the root layer and the second layer in Fig. 11d, the sidewall penetration and the HAZ width are obviously smaller for the second layer. This is because three sides need to be melted during the second layer welding. There are two main explanations for how the GTA can solve these problems. One is that the arc pressure of the GTA can directly pushes the liquid metal towards the sidewalls [16], forming the favorable weld bead formation. The other reason is that the GTA inputs extra heat in the weld pool, which can enhance the fluidity of the liquid metal [17].

3.3.2 Effect of the GTA on microstructure and hardness

Figure 12 shows the microstructure when a GTA is added to the TW-GIA. Comparative images of the microstructure are shown in Figs. 8b and 9b, which are generated by the TW-GIA without a GTA. Figure 12a, b is the FZ and HAZ microstructure of the root layer. It shows that they mostly consist of ferrite and pearlite, and the crystal grains are in columnar shape in the FZ and granular shape in HAZ. Compared with the microstructure without a GTA, apparently, the grain size

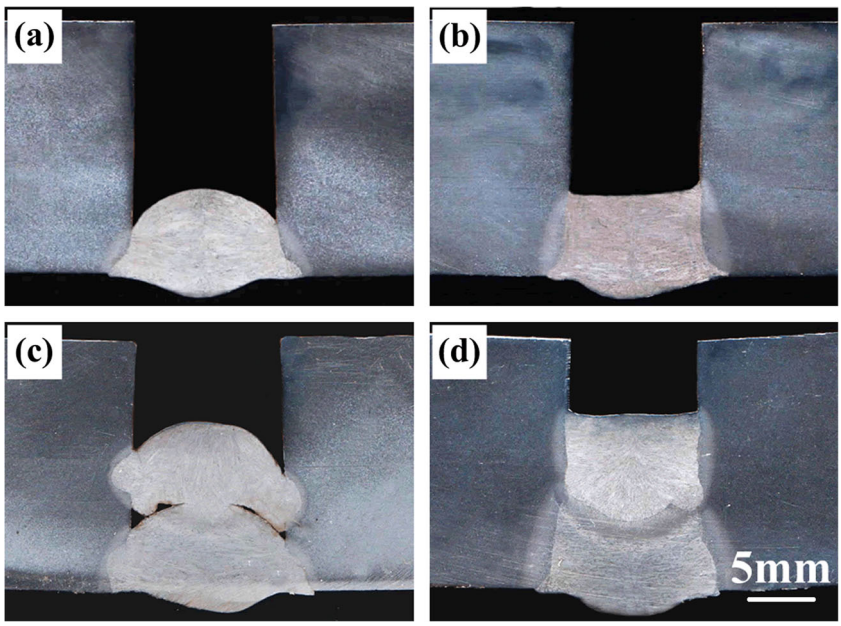

Fig. 11 Cross-section of the weld bead with and without GTA

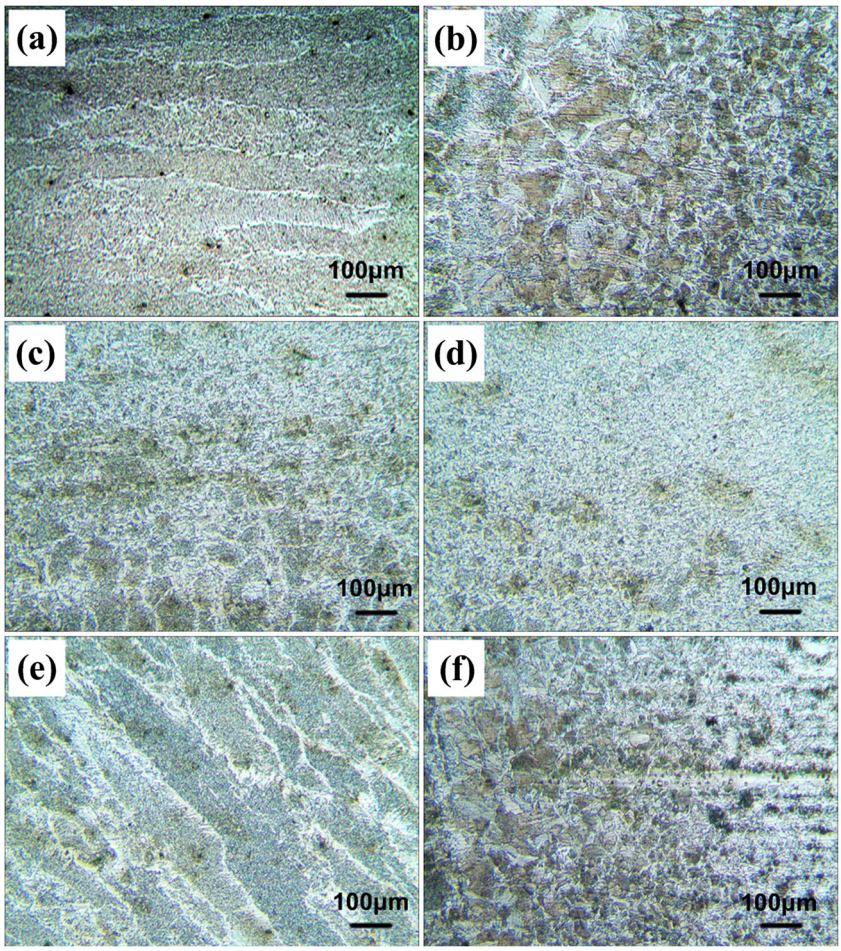

Fig. 12 Microstructure of the weld bead with a GTA behind TW-GIA

coarsens with a GTA. Figure 12c, d is the microstructure of the root layer but affected by the second layer. It shows that there are coarse grains and fine grains indicated by Fig. 12c, d, respectively. Figure 12e, f is the microstructure of the second layer. Compared with the microstructure of the root layer, it shows that the grain size both at the FZ and the HAZ is smaller in the second layer.

3.3.3 Mechanical performance

The fractured tensile sample is shown in Fig. 13. It shows that the fracture occurs on the base material indicating achievement of a good mechanical performance of the joint. The yield strength, the ultimate strength, and the elongation are 285 Mpa, 436 Mpa, and 15.2 %, respectively.

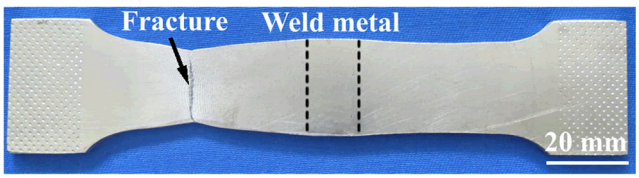

Fig. 13 Fractured tensile test sample

4 Conclusions

(1) Welding currents affect the sidewall penetration more obviously than either the groove gap or the welding speed; as currents increases, sidewall penetration increases. HAZ width is positively related to welding currents and negatively related to groove gap and welding speed. Weld beads tend to form convex surfaces during TW-GIA.

(2) After integrating a GTA with TW-GIA, a concave weld bead surface is obtained, which leads to complete fusion at the weld root for the next weld layer. The GTA also enhances complete fusion between two weld layers. There are two main reasons for this. One is that the arc pressure of the GTA can directly push the liquid metal towards the sidewalls, and the other reason is that the GTA inputs extra heat to the weld pool.

(3) As the welding current increases, the grain size at the FZ and HAZ of the weld bead grows, and the hardness decreases. When a GTA is added to the TW-GIA, the heat input increases, resulting in larger grain size both at the FZ and HAZ compared to the weld bead without a GTA.

References

1. Cui HC, Jiang ZD, Tang XH, Lu FG (2014) Research on narrow-gap GMAW with swing arc system in horizontal position. Int J Adv Manuf Technol 74:297–305
2. Shu FY, Lv YH, Liu YX, Xu FJ, Sun Z, He P, Xu BS (2014) Residual stress modeling of narrow gap welded joint of aluminum alloy by cold metal transferring procedure. Constr Build Mater 54: 224–235
3. Xu WH, Lin SB, Fan CL, Yang CL (2014) Evaluation on microstructure and mechanical properties of high-strength low-alloy steel joints with oscillating arc narrow gap GMA welding. Int J Adv Manuf Technol 75:1439–1446
4. Xu WH, Lin SB, Fan CL, Yang CL (2015) Prediction and optimization of weld bead geometry in oscillating arc narrow gap all-position GMA welding. Int J Adv Manuf Technol 79:183–196
5. Fan CL, Sun QJ, Zhao B, Yang CL, Zhang LF (2009) Stability of double wires narrow gap gas metal arc welding. J Mech E 45(7): 265–269
6. Li WH, Gao K, Wu J, Wang JY, Ji YH (2015) Groove sidewall penetration modeling for rotating arc narrow gap MAG welding. Int J Adv Manuf Technol 78:573–581
7. Guo N, Wang MR, Guo W, Yu JB, Feng JC (2014) Study on forming mechanism of appearance defects in rotating arc narrow gap horizontal GMAW. Int J Adv Manuf Technol 75:15–20
8. Shi CW, Zou Y, Zou ZD, Wu DT (2014) Twin-wire indirect arc welding by modelling and experiment. J Mater Process Tech 214: 2292–2299
9. Fang DS, Song G, Liu LM (2015) A novel method of triple-wire gas indirect arc welding. Mater Manuf Process 31(3):352–358
10. Liu LM, Fang DS, Song G (2015) Experimental investigation of wire arrangements for narrow-gap triple-wire indirect arc welding. Mater Manuf Process. doi:10.1080/10426914.2015.1090603
11. Prasanthi TN, Sudha C, Ravikirana SS, Naveen Kumar N, JanakiRam GD (2015) Friction welding of mild steel and titanium: optimization of process parameters and evolution of interface microstructure. Mater Design 88:58–68
12. Lee HK, Park SH, Kang CY (2015) Effect of plasma current on surface defects of plasma-MIG welding in cryogenic aluminum alloys. J Mater Process Tech 223:203–215
13. Bhargava P, Paul CP, Mundra G, Premsingh CH, Mishra SK, Nagpure D, Kumar A, Kukreja LM (2014) Study on weld bead surface profile and angular distortion in 6 mm thick butt weld joints of SS304 using fiber laser. Opt Laser Eng 53:152–157
14. Xiao WK, Zhu L, Zhang FJ, Dai KS, Zai X, Yang X, Chen BJ (2015) Effect of heat input on cryogenic toughness of 316LN austenitic stainless steel NG-MAG welding joints with large thickness. Mater Design 86:160–167
15. Manti R, Dwivedi DK, Agarwal A (2008) Microstructure and hardness of Al-Mg-Si weldments produced by pulse GTA welding. Int J Adv Manuf Technol 36:263–269
16. Wu CS, Hu ZH, Zhong LM (2012) Prevention of humping bead associated with high welding speed by double-electrode gas metal arc welding. Int J Adv Manuf Technol 63:573–581
17. Yang MX, Yang Z, Qi BJ (2015) Effect of fluid in molten pool on the welds with Ti-6Al-4V during pulsed arc welding. Int J Adv Manuf Technol 81:1007–1016